ADVANCED MATERIALS TECHNOLOGIES
www.advmattechnol.de

3D Inkjet Printing of Electronics Using UV Conversion

Ehab Saleh, Fan Zhang, Yinfeng He, Jayasheelan Vaithilingam, Javier Ledesma Fernandez, Ricky Wildman, Ian Ashcroft, Richard Hague, Phill Dickens, and Christopher Tuck*

The production of electronic circuits and devices is limited by current manufacturing methods that limit both the form and potentially the performance of these systems. Additive manufacturing (AM) is a technology that has been shown to provide cross-sectoral manufacturing industries with significant geometrical freedom. A research domain known as multifunctional AM (MFAM) in its infancy looks to couple the positive attributes of AM with application in the electronics sector can have a significant impact on the development of new products; however, there are significant hurdles to overcome. This paper reports on the single step MFAM of 3D electronic circuitry within a polymeric structure using a combination of conductive and nonconductive materials within a single material jetting-based AM system. The basis of this breakthrough is a study of the optical absorption regions of a silver nanoparticle (AgNP) conductive ink which leads to a novel method to rapidly process and sinter AgNP inks in ambient conditions using simple UV radiation contemporaneously with UV-curing of deposited polymeric structures.

1. Introduction

Additive Manufacturing (AM), often referred to as 3D Printing, has recently proliferated in a wide range of applications for polymer and metallic materials owing to the significant increased geometrical complexity available when compared to traditional production methods.[1–6] The applicability of this disruptive technology to a wide range of industrial sectors has also seen a burgeoning research interest including increases in speed, material qualification, design systems, and application development. However, a step change in part functionality can also be achieved through the extension of AMs inherent flexibility that stems from its layer-by-layer nature. This extension comes from the ability to combine vastly different materials within the deposition of a layer. The combination of these dissimilar materials brings additional research challenges, namely in their deposition, conversion, and interfaces. The opportunity for AM more generally has been determined by its functionality over more traditional manufacturing methods; where geometrical complexity is an inherent strength. The realization of multifunctional AM (MFAM) could augment this opportunity through the processing of multiple materials to gain further component function in the final part.[7–12] Previous work in multiple material deposition has focused on the grading of materials to enhance physical, mechanical, and biological characteristics.[4,5,13] However, the concurrent deposition of dissimilar materials is in its infancy, due in the main to the disparate materials processing requirements for metals, polymers, and ceramics.

In general the 3D printing of electronic structures is dominated by the conformal printing of conductive materials onto the surface of a dielectric structure (otherwise known as Direct Write),[14–18] or the embedment of conductive elements within previously 3D-printed dielectric materials.[19–22] Other reports have demonstrated the printing of conductive, semi-conductive and dielectric materials in a single component, but these were limited to a small number of layers (<10 layers) and hence vertical heights of a few 100 µm, limiting the aspect ratio of these 3D conductive structures.[20,23–26] A commercial product, Voxel 8, was recently launched to extrude conductive pastes and thermal plastics in a single 3D printing apparatus.[27] This approach shows that the 3D printing of functional tracks is possible but the method is often limited by the low spatial resolution of the process being used (e.g., extrusion-based AM).

Recently, inkjet printing has been used for the deposition of a wide range of functional inks with a diverse spectrum of properties.[26,28–32] The fact that inks are ejected from print heads with a large number of small nozzles offers scalability through a droplet on demand (DoD) regime, one that is commonly enabled through piezoelectric inkjet print technology. This regime is key to enable the deposition of different materials alongside each other, required for MFAM. DoD inkjet printing has been reported as a tool for multimaterial fabrication due to the flexibility of the technology to dynamically adapt different patterns and materials in contrast to other printing and manufacturing technologies that require fixed mask or tooling. DoD technology is being applied in a diverse portfolio of applications, for example in biology, tissue bioprinting, multienzyme inkjet printing, and various types of cell printing have been recently reported.[13,33–36] In electronics, a wide range of inkjet-printed applications have been demonstrated, ranging from inkjet printing of passive components,[37–40] active components (e.g.,

Dr. E. Saleh, Dr. F. Zhang, Dr. Y. He, Dr. J. Vaithilingam,
J. L. Fernandez, Prof. R. Wildman, Prof. I. Ashcroft,
Prof. R. Hague, Prof. P. Dickens, Prof. C. Tuck
Centre for Additive Manufacturing
University of Nottingham
Nottingham NG7 2RD, UK
E-mail: Ehab.Saleh@nottingham.ac.uk

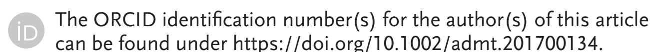
The ORCID identification number(s) for the author(s) of this article can be found under https://doi.org/10.1002/admt.201700134.

© 2017 The Authors. Published by WILEY-VCH Verlag GmbH & Co. KGaA, Weinheim. This is an open access article under the terms of the Creative Commons Attribution License, which permits use, distribution and reproduction in any medium, provided the original work is properly cited.
The copyright line of this paper was changed 21 September 2017 after initial publication.

DOI: 10.1002/admt.201700134

transistors and logic circuits),[20,23,25,28,41] antennas and electromagnetic responsive materials,[14,42] luminance devices,[43–45] and various types of sensing applications.[46–49] These applications highlight the flexibility and potential of the technique; however, it should be pointed out that many of these applications either used a single material printing technique or have been achieved in a small number of layers forming 2D structures and do not take advantage of the 3rd dimension.

The common methodology for device production reported in these studies is to use multiple processes of fabrication because of the differing requirements for deposition, this includes aspects such as viscosity and surface tension limits, the size of functional particles and their requirements for ink solidification from the liquid state. This multiprocess approach is a challenge when aiming to produce 3D-printed parts of multiple materials because of the need to change the printing and ink solidification methods both on an intra and interlayer basis for each material, rendering the process slow and impractical when hundreds or thousands of layers are needed to form an object.

An alternative approach to produce combined conductive and nonconductive printed objects in a single curing process is to embed conductive nanoparticles into UV curable polymers to initiate a percolation of conductive paths.[50] Although this process simplifies the processing requirements it has significant deleterious effects on the final electrical properties of the deposited structure such as reduced conductivity, limiting the final use of the components being manufactured.[50,51]

This paper combines the disciplines of 2D printed electronics with AM to expand the impact of MFAM. It shows that it is possible to overcome some of the major research challenges in the 3D-printing of highly dissimilar multimaterial structures. These challenges include the postdeposition material conversion steps and the complex apparatus required to rapidly sinter the conductive deposits. This paper serves to prove the hypothesis that UV irradiation can be used for the contemporaneous conversion of inkjet-printed UV curable polymeric materials into functional artifacts and the sintering of inkjet-printed silver nanoparticle (AgNP) materials into functional electronic tracks. This will be achieved through understanding the absorption and processing characteristics of the individual materials, demonstration of their simultaneous printing and conversion and finally combination of these techniques into a physical demonstrator.

2. UV Sintering of Silver Nanoparticles Ink

The 3D inkjet printing of dielectric polymeric inks has been studied thoroughly and are commercially available using UV curing techniques.[52,53] The most commonly available conductive inks, such as those consisting of silver, copper, and carbon precursors[29,54–58] consist of nanoparticulate dispersions in carrier solvents with additives such as surfactants to manage agglomeration and viscosity modifiers to tune the viscosity of the ink. When an ink is deposited onto the surface of a substrate the deposit requires evaporation of the carrier solvent, leaving behind the functional nanoparticles for final sintering onto the substrate.[29,55] This evaporation/sintering process is normally performed ex situ within a temperature range of between 100 and 500 °C and usually takes around 15 min per layer using conventional ovens and similar heat sources.[29,54–56] This is significant since the final sintered layer thickness of a commercial silver ink is between 0.5 and 1 µm, and as a consequence producing a macrosized objects (e.g., >1 mm in height) becomes infeasible due to the repeated postprocessing times required between layers. This is contrasted and compounded by the relative efficiency of printing UV curable polymeric materials where individual layers of cured material are of the order of 10 µm in thickness and are often polymerized in seconds.

Despite this apparent difficulty in processing conductive materials, there are still significant benefits of ink jet printing, particularly if the postdeposition processing can be accelerated; ink jet printing is inherently scalable and when deposition of multiple materials is done contemporaneously it offers the possibility for complex properties.

2.1. Hypothesis of UV Sintering

A method of improving the efficiency of postdeposition processing has come about in recent years, based on a photothermal mechanism and is known as intense pulsed light (IPL). IPL has been used to demonstrate a photothermal sintering mechanism for inkjet-printed conductive inks, providing high conductivities from a few tens of pulses each of a few milliseconds in duration.[59–63] Short intense pulses are flashed on to the printed ink using high power xenon lamps. This heats the deposited material through photonic absorption and indirectly generates rapid localized heat. Although effective, if it is not well-controlled IPL can lead to a destruction of the printed tracks owing to extreme rapid heating and cooling.[61,62] These IPL units use the spectral emission of Xenon lamps ranges from 200 to 800 nm wavelengths with a peak intensity between 500 and 700 nm[60,61] making it ideal for copper nanoparticle inks that have their highest absorption peak at around 600 nm.[61,64–66] However, the absorption peaks of silver nanoparticle inks are around 400 nm[60,61,64–66] hence using IPL from Xenon lamps would use a relatively narrow band of the xenon lamp emission that overlaps with the AgNP absorption band.

Sintering of silver nanoparticle inks in the UV range has been reported as an assistive method using conventional heat treatment in addition to UV irradiation to enhance the conductivity but not as a stand-alone sintering technique.[61,62,67] Wunscher et al. reported that UV irradiation on its own is not sufficient to convert metal nanoparticle inks into a conductive counterpart.[61] This is the case for copper nanoparticle inks which have an absorption peak at around 600 nm, but for silver nanoparticle inks containing particles <50 nm in diameter, (as shown in **Figure 1**A,B), the absorption peaks are within the UV range and merge to the visible wavelengths in the range of 380–420 nm (Figure 1C), hence UV irradiation in the range of 390 nm wavelength could be a suitable and efficient method to sinter silver nanoparticle inks as a stand-alone technique.

UV sintering of silver nanoparticle inks as an assistive technique was also reported by Polzinger et al.[67] Polzinger printed silver nanoparticle inks on a heated substrate at 100 °C and used an UV (200–400 nm) oven operating with a power density of 80 W cm^{-1} to enhance the conductivity of the deposit.

© 2017 The Authors. Published by WILEY-VCH Verlag GmbH & Co. KGaA, Weinheim

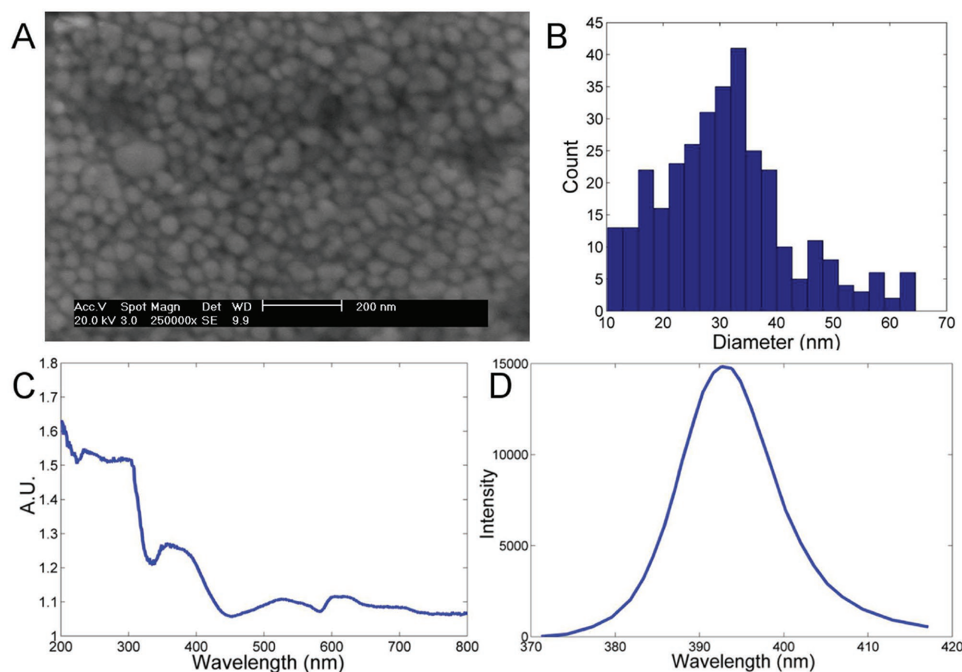

Figure 1. A) FE-SEM image of unprocessed ANP silver nanoparticle ink. B) Size distribution of the nanoparticles computed from FE-SEM images. C) UV–vis spectrum of ANP silver nanoparticle ink. D) Emission spectrum of the LED-based UV light source.

Polzinger achieved a resistivity around 6.5 µΩ cm after 80 s of UV exposure; however, the mechanism of the resulting enhancement of conductivity was not explained.

2.2. Tuning the Sintering Wavelength for a Silver Nanoparticle Ink

A requirement for efficient sintering is that the photonic source wavelength is matched to the spectral absorption peaks of the silver ink. A silver nanoparticle ink from advanced nanoproducts (ANP) was used as a test ink and consisted of 38.85 wt% of silver nanoparticles dispersed in triethylene glycol monomethyl ether (TGME). This silver ink showed high stability during printing due to the presence of well-dispersed nanoparticles and the low vapor pressure of TGME that evaporates relatively slowly and prevents drying of the ink on the print-head nozzle plate. The low vapor pressure whilst offering stability during printing results in slow evaporation of the solvent postdeposition, leading to extended postprocessing time using conventional heat sources.

The size of the silver nanoparticles used in the ANP ink was analyzed using a field emission scanning electron microscope (FE-SEM). Figure 1A shows an FE-SEM image of the nanoparticles prior to sintering, and Figure 1B shows the size distribution of the silver nanoparticles computed through image analysis of the FE-SEM data.

Silver nanoparticles below 50 nm in diameter are reported to have wavelength absorption regions below 430 nm and an absorption peak at around 400 nm with strong dependency on the particle size.[60,61,64–66] UV–vis absorption spectra of the ANP ink showed two absorption regions: one below 310 nm and the second between 330 and 430 nm as shown in Figure 1C.

The main regions of significant absorption in the UV–vis spectrum of the major component within the carrier fluid (TGME) were below 300 nm (Figure S2, Supporting Information), therefore the first absorption region of the AgNP ink below 310 nm is likely to be due to the presence of organic additives (surfactant, viscosity modifiers) in the ink, while the second peak of 330–430 nm a result of the silver nanoparticles absorption in line with previous reports.[60,61,64–66]

3. Development and UV Curing of a Dielectric Ink

To provide structure and a nonconductive layer, a tri(propylene glycol) diacrylated (TPGDA) material was developed as described in the Methods section of the Supporting Information. TPGDA has been used in previous studies[68–70] to produce organic thin-film transistors through a vacuum flash-evaporation process and cured by electron beam. As TPGDA contains photosensitive acrylate groups, the curing reaction can also be initiated under UV light with the presence of proper photoinitiators through the free-radical photopolymerization.[71]

4. Inkjet Printing and UV Sintering Apparatus

A light emitting diode (LED)-based UV source was used for all processing experiments, chosen because of the efficiency of LED technology when compared to Mercury vapor UV sources or Xenon lamps as well as the relatively compact size of LED sources. The LED-based UV unit had an emission peak at 395 nm with a full width at half maximum wavelength of 386–401 nm (Figure 1D). The optical power density from the UV source was found to be 0.557 W cm^{-2} at a distance of 4 mm

 © 2017 The Authors. Published by WILEY-VCH Verlag GmbH & Co. KGaA, Weinheim

from the UV light. The ANP silver ink was inkjet printed by a Spectra SE128 print-head installed into a PixDro LP50 printer, the UV light was installed on the print-head assembly at a distance of 70 mm away from the print head in the direction of printing (**Figure 2**).

The printer was programmed to illuminate with UV light after a layer was printed. In order to understand the required energy delivery for sintering the AgNP ink, tracks of 0.5 mm × 5 mm (width × length mm^2) were printed on borosilicate glass slides.

The height between the UV light and the substrate was fixed at 4 mm. Each track of AgNP ink was printed under ambient conditions and then UV sintered for different time periods at a fixed UV power. To evaluate the sintering conditions the resistivity of each UV-sintered track was measured and plotted against the energy delivered ($E = t_s.P_i$) to the ink tracks, where t_s represents the time of sintering and P_i the UV incident power density at deposition (**Figure 3**A). To measure the resistivity of each track the resistance was measured using a Hameg LCR high precision meter. The volume of the deposited and sintered tracks was measured by integrating surface profiles measured using white light interferometer (Bruker ContourGT).

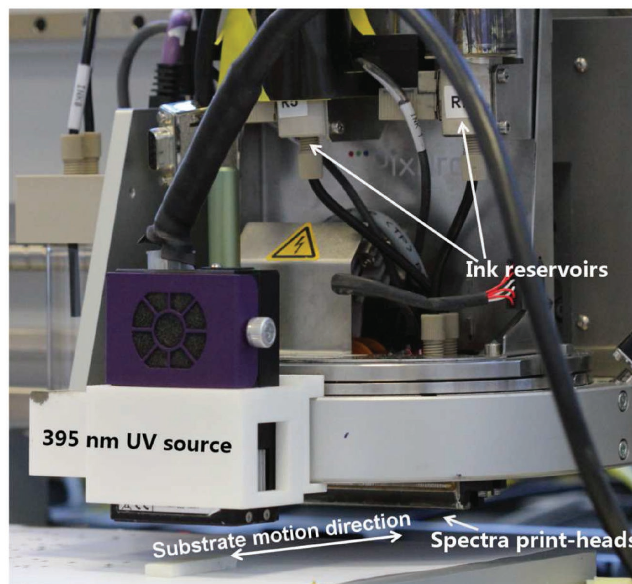

Figure 2. Printing apparatus with UV installed on the print-head assembly.

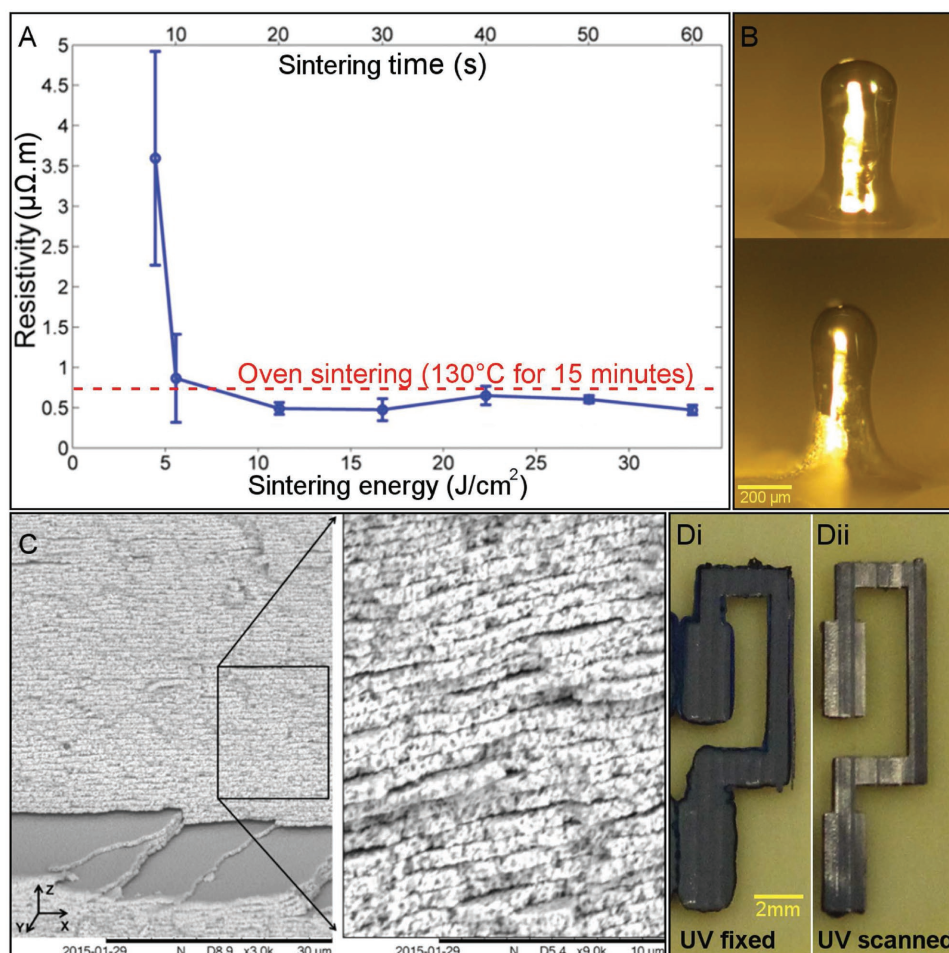

Figure 3. A) Track resistivity characterization of the UV sintered silver ink with changes in UV irradiation energy. B) Samples of silver columns printed and UV sintered for *z*-direction resistivity measurements. C) Layering effect appears when printing multiple layers of UV sintered silver ink. D) Bulging of ink when the UV source is at fixed position over the pattern compared to scanning the UV over the entire pattern.

© 2017 The Authors. Published by WILEY-VCH Verlag GmbH & Co. KGaA, Weinheim

Tuning the sintering wavelength to the absorption peaks of the silver ink resulted in low energy requirements to sinter the ink from the "wet" droplet state using the low power UV light source. This is evident when the same dimensions of the silver ink was sintered in a conventional oven for 15 min at 130 °C as recommended by the ink supplier where UV sintering has shown lower resistivity. To quantify the efficiency of the sintering mechanism a Figure of merit (ρE) was introduced to evaluate future photothermal sintering attempts. The Figure of merit represents the resistivity of the sample (ρ), the sintering time (t_s), and the UV incident power density (P_i) as shown in Equation (1)

$$\rho E = \rho . t_s . P_i \quad (1)$$

The higher the efficiency of the sintering process the lower the value of the figure of merit, which requires lower values of the sintering time, the incident power or the resistivity. For the current study after 10 s of UV exposure the figure of merit (ρE) was 4.81 μΩ m J cm^{-2} for the most efficient sintering conditions.

At low UV energy below 5 J cm^{-2} a high level of variability appears which is likely to be due to incomplete sintering of the AgNP in the tracks indicating that a number of the nanoparticles were not contributing to the percolation within the track.

To measure the resistivity of the UV sintered AgNP ink in the z direction columns of 1000 layers were printed and UV sintered for 30 s per layer at 0.557 W cm^{-2} UV power density. The resistance of the columns was measured between two copper probes (2 mm thick in each case) to reduce the influence of the wiring on the total resistance (see the Supporting Information).

The dimensions of the pillars were around 150–200 μm in diameter and 450–500 μm in height (Figure 3B). The resistivity of the stacked pillars in the z direction was 7.1 ± 1.4 μΩ m, an order of magnitude higher than the x–y direction resistivity. To understand the difference between x–y direction resistivity and the z direction resistivity a square 5 mm × 5 mm was printed and UV sintered with the same conditions as the pillars then analyzed in a cross-sectional orientation with SEM (Figure 3C).

The thickness of each UV sintered silver layer in Figure 3C ranges from 500 to 800 nm correlating to the surface profile data collected for measuring the resistivity. This layering effect explains the difference between the x–y direction resistivity and the z direction resistivity, where dark barrier areas appear between the layers in the z direction but not in the x–y direction. Energy-dispersive X-ray spectroscopy (EDX) was conducted to analyze the composition of the stacked samples. EDX showed fine traces of carbon in the dark areas between the layers which indicates the presence of organic residue. This may be from the dispersant and other organic additives within the ink, which have migrated to the surface during the sintering process but did not decompose or form voids between the layers.

Large deposition areas in comparison to the spot of the UV source showed a bulging effect (Figure 3Di). This could be in part due to the UV intensity profile from the center of the spot toward the edges, i.e., due to the high intensity of light at the center of the UV spot AgNP ink at the center of the deposition area absorbs the higher intensity UV light, generating more heat than at the edges; therefore a Marangoni effect occurs where ink from the hotter areas in the center flows toward the colder edges. To overcome the bulging effect the UV source was scanned over the deposition to cover the entire area equally and prevents focusing the UV spot at the center of the deposition. Effective scanning speeds were in the range of 100–150 mm s^{-1}. By scanning the entire area the heat generated within the sample will not be focused at the center of the deposition minimizing the Marangoni effect, also as the UV spot is scanned over the edges it will cause a pinning effect to occur at the edges of the deposited area further preventing the bulging from occurring.[72]

5. Demonstrations of Multimaterial Printing

The conductive ink (ANP) and the dielectric UV curable ink (TPGDA) were loaded into reservoirs connected to two spectra print-heads as shown in Figure 2. The dielectric ink was printed and cured in real time through UV irradiation over the sample after each jetting pass or swathe. This swathe by swathe curing was able to produce fine polymeric surfaces (as shown in **Figure 4**). The silver ink was sintered by scanning the UV light over the deposit after each layer was completed.

In order to sinter and cure the conductive and dielectric inks in a single process it was necessary to evaluate the influence of the UV irradiation on both materials. UV–vis spectroscopy was conducted on the dielectric ink to verify its absorption peaks as shown in Figure S4 in the Supporting Information. The UV cured ink showed low absorption in the visible region 400–700 nm. The narrow overlap between the emission of the UV light and the low absorption of the dielectric ink was also observed. When silver ink is printed on top of a printed dielectric layers the UV sintering requirements of the silver ink were lower as the cured dielectric ink was mildly contributing to the absorption of the UV light (see Figure S4, Supporting Information).

Various shapes were demonstrated using conductive and dielectric inks as shown in Figure 4. More detail about the production of these parts is available in Movies S1 and S2 in the Supporting Information.

The work presented in this paper highlights that the ability to 3D print electronic circuits which can be achieved using relatively inexpensive UV light sources coupled to piezo-based inkjet deposition systems. In addition, standard nanoparticulate materials normally reserved for 2D printed electronics can be utilized negating the need to modify and develop new ink formulations to demonstrate the concept of multimaterial AM electronics. This final remark is important as the realization of this technology could yield significant uptake for those interested in producing optimal geometric structures for example, 3D antenna[14,73] or radiofrequency (RF) metamaterials[74,75] without significant compromise on material performance.

6. Conclusion

In this study, the optical properties of a silver nanoparticle ink used for inkjet printing have been characterized and used to inform a novel sintering protocol based on light absorption.

© 2017 The Authors. Published by WILEY-VCH Verlag GmbH & Co. KGaA, Weinheim

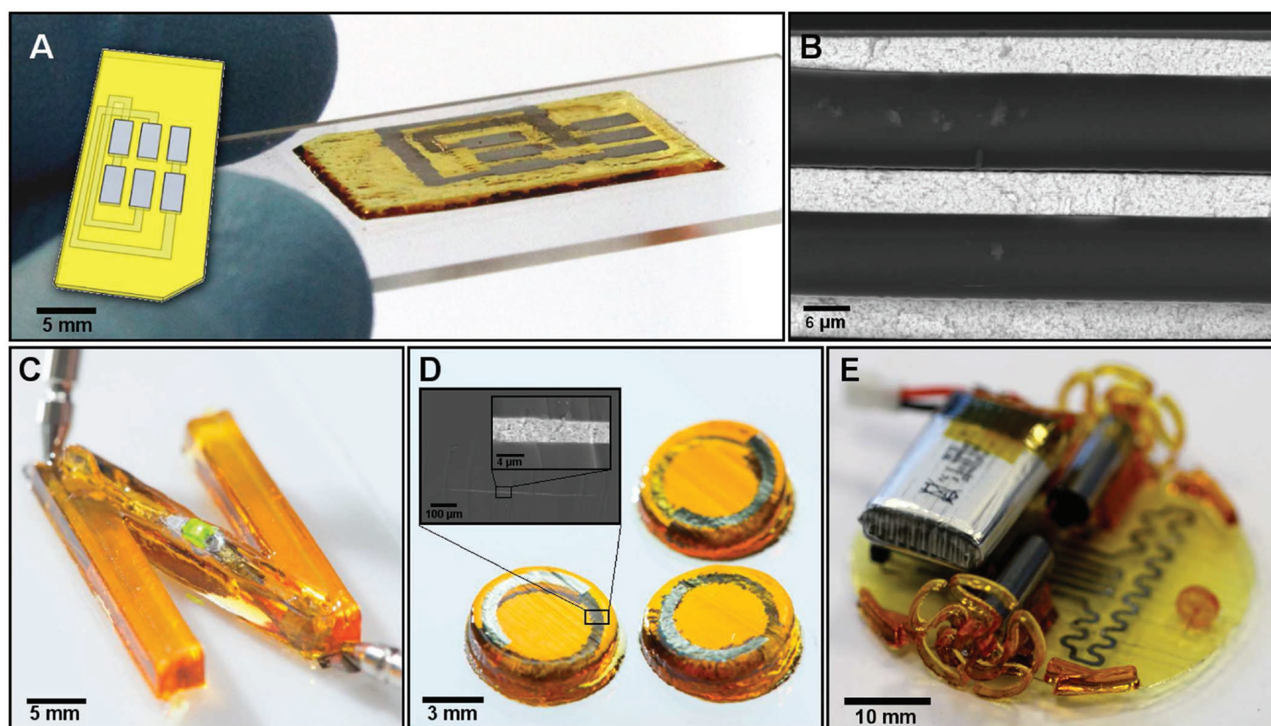

Figure 4. Macro- and microdemonstrators of polymeric and metallic materials printed in one structure. A) Conductive and dielectric inks printed and UV irradiated forming security chip with specific conductive layout. B) SEM image of a cross-section of UV sintered silver tracks (bright lines) encapsulated within UV cured polymeric ink (dark lines). C) Letter N shape printed using conductive tracks within a 3 mm thick dielectric pattern connecting an LED to a power source. D) Helix tracks printed within dielectric tube structure. E) 3D printed two-wheeled robotic car with strain sensing shape tracks printed and encapsulated within the base of the car.

The strong absorption peaks in the UV range were used to select a light source with matching emission peaks to irradiate the nanoparticle-based ink in order to initiate a photothermal sintering process. Instead of irradiating the ink with high power and broad wavelength light, as is usually done in photothermal sintering processes, a low power UV light source with a wavelength of 395 nm was selected and used throughout.

The photothermal sintering process was able to convert the silver nanoparticle ink into solid conductive films from the liquid phase eliminating the need for pre or postheating processes. This vastly speeds up the sintering process and enables the fabrication of large number of layers which was traditionally limited due to the different and involved postprocesses required.

Sintered conductive tracks showed an average planer resistivity of 0.48 $\mu\Omega$ m after 30 s of UV irradiation which was lower than the resistivity of the same ink after 15 min of oven sintering at 130 °C as recommended by the ink supplier.

The durable LED-based UV light was inexpensive, compact, efficient, and able to photocure polymers alongside sintering the conductive inks which has enabled an unprecedented fabrication capability of 3D macro- and microstructures which contain multimaterials using one apparatus.

Supporting Information

Supporting Information is available from the Wiley Online Library or from the author.

Acknowledgements

This work was supported by the Engineering and Physical Sciences Research Council [grant number EP/I033335/2] under the EPSRC Centre for Innovative Manufacturing in Additive Manufacturing at the University of Nottingham, and the EPSRC Jetting Electronic Tracks JET project.

Conflict of Interest

The authors declare no conflict of interest.

Keywords

additive manufacturing, conductive ink, polymeric ink, UV sintering

Received: May 19, 2017
Published online: August 17, 2017

[1] E. MacDonald, R. Wicker, *Science* **2016**, *353*, , 1512.
[2] A. Panesar, D. Brackett, I. Ashcroft, R. Wildman, R. Hague, *J. Mech. Des.* **2015**, *137*, 111414.
[3] R. D. Goodridge, C. J. Tuck, R. J. M. Hague, *Prog. Mater. Sci.* **2012**, *57*, 229.
[4] J. R. Tumbleston, D. Shirvanyants, N. Ermoshkin, R. Janusziewicz, A. R. Johnson, D. Kelly, K. Chen, R. Pinschmidt, J. P. Rolland,

 © 2017 The Authors. Published by WILEY-VCH Verlag GmbH & Co. KGaA, Weinheim

A. Ermoshkin, E. T. Samulski, J. M. DeSimone, *Science* **2015**, *347*, 1349.
[5] I. Maskery, A. Hussey, A. Panesar, A. Aremu, C. Tuck, I. Ashcroft, R. Hague, *J. Cell. Plast.* **2017**, *53*, 151.
[6] G. A. T. Sevilla, M. D. Cordero, J. M. Nassar, A. N. Hanna, A. T. Kutbee, A. Arevalo, M. M. Hussain, *Adv. Mater. Technol.* **2017**, *2*, 1600175.
[7] D. Espalin, D. W. Muse, E. MacDonald, R. B. Wicker, *Int. J. Adv. Manuf. Technol.* **2014**, *72*, 963.
[8] M. Liang, C. Shemelya, E. MacDonald, R. Wicker, H. Xin, *IEEE Antennas Wireless Propag. Lett.* **2015**, *14*, 1346.
[9] M. S. Mannoor, Z. Jiang, T. James, Y. L. Kong, K. A. Malatesta, W. O. Soboyejo, N. Verma, D. H. Gracias, M. C. McAlpine, *Nano Lett.* **2013**, *13*, 2634.
[10] Y. L. Kong, I. A. Tamargo, H. Kim, B. N. Johnson, M. K. Gupta, T.-W. Koh, H.-A. Chin, D. A. Steingart, B. P. Rand, M. C. McAlpine, *Nano Lett.* **2014**, *14*, 7017.
[11] Y. L. Kong, M. K. Gupta, B. N. Johnson, M. C. McAlpine, *Nano Today* **2016**, *11*, 330.
[12] G. A. T. Sevilla, M. M. Hussain, *IEEE J. Emerging Sel. Top. Circuits Syst.* **2017**, *7*, 147.
[13] B. Derby, *Science* **2012**, *338*, 921.
[14] J. J. Adams, E. B. Duoss, T. F. Malkowski, M. J. Motala, B. Y. Ahn, R. G. Nuzzo, J. T. Bernhard, J. A. Lewis, *Adv. Mater.* **2011**, *23*, 1335.
[15] J. A. Lewis, B. Y. Ahn, *Nature* **2015**, *518*, 42.
[16] E. Macdonald, R. Salas, D. Espalin, M. Perez, E. Aguilera, D. Muse, R. B. Wicker, *IEEE Access* **2014**, *2*, 234.
[17] J. M. Nassar, M. D. Cordero, A. T. Kutbee, M. A. Karimi, G. A. T. Sevilla, A. M. Hussain, A. Shamim, M. M. Hussain, *Adv. Mater. Technol.* **2016**, *1*, 1600004.
[18] J. M. Nassar, K. Mishra, K. Lau, A. A. Aguirre-Pablo, M. M. Hussain, *Adv. Mater. Technol.* **2017**, *2*, 1600228.
[19] D. Espalin, D. Muse, E. MacDonald, R. Wicker, *Int. J. Adv. Manuf. Technol.* **2014**, *72*, 963.
[20] A. C. Arias, S. E. Ready, R. Lujan, W. S. Wong, K. E. Paul, A. Salleo, M. L. Chabinyc, R. Apte, R. A. Street, Y. Wu, P. Liu, B. Ong, *Appl. Phys. Lett.* **2004**, *85*, 3304.
[21] S. Yao, Y. Zhu, *Nanoscale* **2014**, *6*, 2345.
[22] S.-Y. Wu, C. Yang, W. Hsu, L. Lin, *Microsyst. Nanoeng.* **2015**, *1*, 15013.
[23] K. E. Paul, W. S. Wong, S. E. Ready, R. A. Street, *Appl. Phys. Lett.* **2003**, *83*, 2070.
[24] L. Yun, S. Huabin, S. Yi, T. Kazuhito, *Sci. Technol. Adv. Mater.* **2014**, *15*, 024203.
[25] D. Tobjörk, N. J. Kaihovirta, T. Mäkelä, F. S. Pettersson, R. Österbacka, *Org. Electron.* **2008**, *9*, 931.
[26] H. K. Seung, P. Heng, P. G. Costas, K. L. Christine, M. J. F. Jean, P. Dimos, *Nanotechnology* **2007**, *18*, 345202.
[27] Voxel8 Inc., http://www.voxel8.co/case-studies/ (accessed: March 2017).
[28] H. Sirringhaus, T. Kawase, R. H. Friend, T. Shimoda, M. Inbasekaran, W. Wu, E. P. Woo, *Science* **2000**, *290*, 2123.
[29] P. J. Smith, D. Y. Shin, J. E. Stringer, B. Derby, N. Reis, *J. Mater. Sci.* **2006**, *41*, 4153.
[30] B. Derby, *Annu. Rev. Mater. Res.* **2010**, *40*, 395.
[31] A. L. Dearden, P. J. Smith, D.-Y. Shin, N. Reis, B. Derby, P. O'Brien, *Macromol. Rapid Commun.* **2005**, *26*, 315.
[32] E. Saleh, P. Woolliams, B. Clarke, A. Gregory, S. Greedy, C. Smartt, R. Wildman, I. Ashcroft, R. Hague, P. Dickens, C. Tuck, *Addit. Manuf.* **2016**.
[33] S. V. Murphy, A. Atala, *Nat. Biotechnol.* **2014**, *32*, 773.
[34] B. Lorber, W.-K. Hsiao, I. M. Hutchings, K. R. Martin, *Biofabrication* **2014**, *6*, 015001.
[35] Y. Zhang, F. Lyu, J. Ge, Z. Liu, *Chem. Commun.* **2014**, *50*, 12919.
[36] P. Calvert, *Science* **2007**, *318*, 208.
[37] T. Kawase, H. Sirringhaus, R. H. Friend, T. Shimoda, *Adv. Mater.* **2001**, *13*, 1601.
[38] S. H. Ko, J. Chung, H. Pan, C. P. Grigoropoulos, D. Poulikakos, *Sens. Actuators, A* **2007**, *134*, 161.
[39] B. J. Kang, C. K. Lee, J. H. Oh, *Microelectron. Eng.* **2012**, *97*, 251.
[40] B. Chen, T. Cui, Y. Liu, K. Varahramyan, *Solid-State Electron.* **2003**, *47*, 841.
[41] S. Conti, S. Lai, P. Cosseddu, A. Bonfiglio, *Adv. Mater. Technol.* **2017**, *2*, 1600212.
[42] E. Saleh, C. Tuck, C. Thiantanukij, P. Woolliams, B. Clarke, R. Wildman, I. Ashcroft, R. Hague, P. Dickens, *International Symposium on Flexible Automation*, Japan **2014**, p. 94L.
[43] E. Tekin, E. Holder, V. Marin, B.-J. de Gans, U. S. Schubert, *Macromol. Rapid Commun.* **2005**, *26*, 293.
[44] H. Zheng, Y. Zheng, N. Liu, N. Ai, Q. Wang, S. Wu, J. Zhou, D. Hu, S. Yu, S. Han, W. Xu, C. Luo, Y. Meng, Z. Jiang, Y. Chen, D. Li, F. Huang, J. Wang, J. Peng, Y. Cao, *Nat. Commun.* **2013**, *4*, 2971.
[45] H. M. Haverinen, R. A. Myllyla, G. E. Jabbour, *J. Disp. Technol.* **2010**, *6*, 87.
[46] J. Kukkola, M. Mohl, A.-R. Leino, G. Toth, M.-C. Wu, A. Shchukarev, A. Popov, J.-P. Mikkola, J. Lauri, M. Riihimaki, J. Lappalainen, H. Jantunen, K. Kordas, *J. Mater. Chem.* **2012**, *22*, 17878.
[47] N. Komuro, S. Takaki, K. Suzuki, D. Citterio, *Anal. Bioanal. Chem.* **2013**, *405*, 5785.
[48] B. Ando, S. Baglio, *Sens. J. IEEE* **2013**, *13*, 4874.
[49] F. Molina-Lopez, D. Briand, N. F. de Rooij, *Sens. Actuators, B* **2012**, *166*, 212.
[50] A. Chiolerio, L. Vescovo, M. Sangermano, *Macromol. Chem. Phys.* **2010**, *211*, 2008.
[51] M. Sangermano, A. Chiolerio, G. Marti, P. Martino, *Macromol. Mater. Eng.* **2013**, *298*, 607.
[52] S. Velankar, J. Pazos, S. L. Cooper, *J. Appl. Polym. Sci.* **1996**, *62*, 1361.
[53] J. Xu, W. Pang, W. Shi, *Thin Solid Films* **2006**, *514*, 69.
[54] J. C. Seung, H. Ko, N. Hotz, K. H. Nam, C. P. Grigoropoulos, *J. Micromech. Microeng.* **2010**, *20*.
[55] B. Y. Ahn, E. B. Duoss, M. J. Motala, X. Guo, S.-I. Park, Y. Xiong, J. Yoon, R. G. Nuzzo, J. A. Rogers, J. A. Lewis, *Science* **2009**, *323*, 1590.
[56] J. Perelaer, P. J. Smith, D. Mager, D. Soltman, S. K. Volkman, V. Subramanian, J. G. Korvink, U. S. Schubert, *J. Mater. Chem.* **2010**, *20*, 8446.
[57] X. Nie, H. Wang, J. Zou, *Appl. Surf. Sci.* **2012**, *261*, 554.
[58] X. Han, Y. Chen, H. Zhu, C. Preston, J. Wan, Z. Fang, L. Hu, *Nanotechnology* **2013**, *24*, 205304.
[59] J. S. Kang, J. Ryu, H. S. Kim, H. T. Hahn, *J. Electron. Mater.* **2011**, *40*, 2268.
[60] Y. Galagan, E. W. C. Coenen, R. Abbel, T. J. van Lammeren, S. Sabik, M. Barink, E. R. Meinders, R. Andriessen, P. W. M. Blom, *Org. Electron.* **2013**, *14*, 38.
[61] S. Wunscher, R. Abbel, J. Perelaer, U. S. Schubert, *J. Mater. Chem. C* **2014**, *2*, 10232.
[62] M. Hosel, F. C. Krebs, *J. Mater. Chem.* **2012**, *22*, 15683.
[63] J. Niittynen, R. Abbel, M. Mäntysalo, J. Perelaer, U. S. Schubert, D. Lupo, *Thin Solid Films* **2014**, *556*, 452.
[64] D. Mau Chien, D. Thi My Dung, F.-B. Eric, *Adv. Nat. Sci.: Nanosci. Nanotechnol.* **2013**, *4*, 015009.
[65] S. L.-C. Hsu, R.-T. Wu, presented at Int. Conf. Nanotechnol. Biosens., *2*, 55–58, Singapore, **2010**.
[66] S. Barcikowski, A. Hahn, A. V. Kabashin, B. N. Chichkov, *Appl. Phys. A* **2007**, *87*, 47.
[67] F. S. B. Polzinger, V. Matic, J. Keck, H. Willeck, W. Eberhardt, H. Kueck, presented at 11th IEEE Int. Conf. Nanotechnol., Oregon, USA Aug. **2011**.

© 2017 The Authors. Published by WILEY-VCH Verlag GmbH & Co. KGaA, Weinheim

[68] G. Abbas, Z. Ding, K. Mallik, H. Assender, D. M. Taylor, *IEEE Electron Device Lett.* **2013**, *34*, 268.
[69] Z. Ding, G. A. Abbas, H. E. Assender, J. J. Morrison, V. Sanchez-Romaguera, S. G. Yeates, D. M. Taylor, *Appl. Phys. Lett.* **2013**, *103*, 233301.
[70] Z. Ding, G. Abbas, H. E. Assender, J. J. Morrison, S. G. Yeates, E. R. Patchett, D. M. Taylor, *ACS Appl. Mater. Interfaces* **2014**, *6*, 15224.
[71] D. Christian, *Pigm. Resin Technol.* **2001**, *30*, 278.
[72] S. Vafaei, C. Tuck, R. Wildman, I. Ashcroft, *Addit. Manuf.* **2016**, *11*, 77.
[73] C. Pfeiffer, X. Xu, S. R. Forrest, A. Grbic, *Adv. Mater.* **2012**, *24*, 1166.
[74] R. A. Shelby, D. R. Smith, S. Schultz, *Science* **2001**, *292*, 77.
[75] D. Schurig, J. J. Mock, B. J. Justice, S. A. Cummer, J. B. Pendry, A. F. Starr, D. R. Smith, *Science* **2006**, *314*, 977.

© 2017 The Authors. Published by WILEY-VCH Verlag GmbH & Co. KGaA, Weinheim